RSC Advances

PAPER

View Article Online
View Journal | View Issue

Cite this: *RSC Adv.*, 2015, **5**, 4872

The effect of titanium in $Li_3V_2(PO_4)_3$/graphene composites as cathode material for high capacity Li-ion batteries†

Mansoo Choi,[ac] Kisuk Kang,[b] Hyun-Soo Kim,[a] Young Moo Lee[c] and Bong-Soo Jin*[a]

Received 10th September 2014
Accepted 1st December 2014

DOI: 10.1039/c4ra09389e

www.rsc.org/advances

We report high capacity and rate capability of titanium-added $Li_3V_2(PO_4)_3$ (LVP) as a cathode material for lithium ion batteries (LIBs). Titanium-added $Li_3V_{2-x}Ti_x(PO_4)_3$/graphene (Ti-added LVP/graphene, $x = 0$, 0.01, 0.03, and 0.05) composites were synthesized through a sol–gel route by using titanium dioxide (TiO_2) and graphene to improve the electrochemical performance. The addition of graphene and titanium significantly enhanced the electric conductivity, resulting in higher kinetic behavior of the LVP. This led to the higher specific capacity of 194 mA h g^{-1} at 0.1 C in the potential range of 3.0–4.8 V. The effect of graphene and Ti atoms in Ti-added LVP/graphene was investigated through physical and electrochemical measurements.

1. Introduction

The paradigm shift in the use of Li-ion batteries (LIBs) has moved from portable devices to higher-volume applications such as electric vehicles' energy storage systems.[1,2] There are still many issues to be resolved before the wide use of LIBs. LIBs should have high energy density, be long-lasting, and cost less. $LiCoO_2$, which is currently used in commercial LIBs, suffers from safety issues and being expensive and toxic.[3,4] Thus, considerable efforts are needed to replace these cathode materials. To date, the transition metal phosphates ($LiMPO_4$, where M = Fe and Mn) discovered by Padhi *et al.* have been regarded as alternative cathode materials owing to their higher capacity, stability and safety.[5–8] Monoclinic $Li_3V_2(PO_4)_3$ (LVP) has also been considered as a potential cathode material because of its high capacity, operating voltage and highly safe performance.[9–12] The Li ions are inserted/extracted through the host framework of $V_2(PO_4)_3$, which consists of the slightly distorted VO_6 octahedra and PO_4 tetrahedra sharing the oxygen vertices. Three lithium ions inserted/extracted from the $V_2(PO_4)_3$ lattice enable the theoretical capacity to achieve 197 mA h g^{-1} in the potential range of 3.0–4.8 V, which is the highest of the polyanion framework materials. In addition, the large polyanion can aid stabilization of the structure and allow fast ion migration.[9,13,14] However, in spite of the advantages of LVP, such as high capacity, safety and environmental compatibility,[15] the development of phosphate-based cathode materials with high energy density is still needed. The low electric conductivity (about 2.3×10^{-8} S cm^{-1} at room temperature) of LVP limits its higher capacity and further practical applications. Over the years, efforts have been devoted to overcoming this obstacle in three ways. First, nano-sized LVP particles are beneficial for improving the electrode kinetics owing to an enhanced reaction interface and decreased diffusion length for both electron and Li ions.[16,17] Second, the method of surface coating with conductive materials has been widely used to improve the intrinsic electric conductivity of LVP cathode materials.[18–21] However, it is difficult to make uniformly a conductive coating layer on active materials. The inhomogeneous surface coating results in a decrease in the charge–discharge capacity at higher current rates because of the lack of the conducting network. Third, transition metal doping is a useful way to improve the electrochemical performance of LVP. Several cations, such as Al^{3+},[22] Fe^{3+},[23] Cr^{3+},[24] Mg^{2+},[25] Co^{2+},[26] and Ti^{4+},[27] doped in the LVP can be replaced at the V site, resulting in improved utilization of materials, high rate capabilities, electric conductivity and cyclic stability. Although there are a lot of reports regarding cation doping in LVP, the discharge capacity at low current density is still lower. So, further work should explore the goal of achieving high LVP capacity.

Graphene, which is a single sheet of carbon atoms packed into a hexagonal lattice, has been considered for improving the electrical performance of LVP, being a great network for an electron path because of its high electrical conductivity, high surface area, good mechanical strength and chemical stability. Even though the LVP/graphene composite has been reported as a cathode material for LIBs,[21,28–30] it required multiple steps for sample preparation and was not suitable for large scale

[a]*Battery Research Center, Korea Electrotechnology Research Institute, Changwon 642-120, Korea. E-mail: bsjin@keri.re.kr*

[b]*Department of Materials Science and Engineering, Seoul National University, Seoul 151-742, Korea*

[c]*Department of Energy Engineering, Hanyang University, Seoul 133-791, Korea*

† Electronic supplementary information (ESI) available. See DOI: 10.1039/c4ra09389e

production. Besides, the large amount of carbon may decrease the volumetric energy density of the electrode. Very recently, we reported a LVP/Ag–graphene composite synthesized by a facile sol–gel route to improve the electric conductivity of the LVP.[31] The LVP/Ag–graphene composites exhibited reasonable discharge capacity at 0.1 C and capacity retention (78%) at 0.5 C in the potential range of 3.0–4.8 V. Moreover, an exceptional discharge capacity of 134 mA h g^{-1} was achieved at 10 C, which is the highest value for graphene-based LVP composites.[21,28–30] Considering our approach for high capacity and rate capability, we have synthesized the Ti-added $Li_3V_{2-x}Ti_x(PO_4)_3$/graphene ($x = 0.01, 0.03, 0.05$) composite through a facile sol–gel method. The effect of graphene and Ti atoms was investigated through physical and electrochemical measurements. The Ti-added LVP/graphene composite did not influence the LVP structure, but it reduced the particle size and improved the electrical conductivity, resulting in high capacity and rate capability.

2. Experimental

All the solvents and chemicals are commercially available and were used as received unless otherwise stated.

2.1 Synthesis of Ti-added LVP/graphene composites

The Ti-added LVP/graphene composites were synthesized through the sol–gel method by using V_2O_5, $C_2H_2O_4$, $NH_4H_2PO_4$, Li_2CO_3, TiO_2 and graphene powder as starting materials. Briefly, V_2O_5 and $H_2C_2O_4$ in a stoichiometric ratio of 1 : 3 were dissolved in deionized (DI) water at 80 °C until a clear blue solution was formed. Oxalic acid was used not only as a reducing agent, but also as a chelating agent. After magnetic stirring for 1 h, the stoichiometric amount of $NH_4H_2PO_4$, Li_2CO_3 and TiO_2 (0.01, 0.03, 0.05 M) was added to the solution, and the mixture was vigorously stirred for 1 h to form the LVP precursor. Hereafter, the $Li_3V_{2-x}Ti_x(PO_4)_3$/graphene ($x = 0$, 0.01, 0.03 and 0.05) will be referred to as pristine LVP, LVP–Ti1, LVP–Ti3 and LVP–Ti5, respectively. Simultaneously, 50 mg of graphene nano-powder was dispersed in another beaker with DI water and then sonicated for 90 min. The LVP precursor solution was poured into the graphene solution and stirred by using a magnetic stirrer for 24 h. The mixture was heated at 80 °C, and the resulting slurry was dried at 100 °C, followed by sintering at 350 °C for 4 h and then 800 °C for 8 h under argon atmosphere in a tube furnace. The ramping rate was 5 °C min^{-1}.

2.2 Physical measurements

The morphology and elements of the samples were investigated by a field emission scanning electron microscopy (FE-SEM, S-4800, Hitachi) working at 30 kV and energy-dispersive spectrum (EDS), respectively. Transition electron microscopy (TEM) images were observed using a TF30ST at a 300 kV acceleration voltage. The powder X-ray diffraction (XRD, X-pert PRO MPD, Philips) patterns of composites were detected with Cu Kα radiation ($\lambda = 1.5406$ Å) operating at 40 kV and 30 mA between 10° and 90° at a scan rate of 0.01°, 2θ min^{-1}. In order to measure the electric conductivity of the electrode, four-probe measurement was used with a Keithley 2400 electrometer. Raman measurement (NTEGRA SPECTRA, NT-MDT) was conducted with a laser wavelength of 532 nm. X-ray photoelectron spectroscopy (XPS, VG Multilab ESCA 2000 system) was employed to measure the chemical or electronic state of each element. The carbon content of the samples was measured by a CHNS Elemental Analyzer (EA, 2400 series 2).

2.3 Electrochemical measurements

The electrochemical performance of the LVP–Ti/graphene was evaluated using 2032 coin cells assembled in a dry room. The electrode was prepared with active material (70%), Super P (20%), and polyvinylidene fluoride (PVdF, 10%) as a binder using *N*-methyl-2-pyrrolidone as a dispersant. Consequently, the paste was casted onto Al foil and dried at 100 °C in a vacuum oven overnight. The Li metal was used as the counter and reference electrode. The 1 M $LiPF_6$ dissolved in ethylene carbonate (EC) and dimethyl carbonate (DMC) (1 : 1 in volume) and polypropylene 2400 were used as electrolyte and separator, respectively. Galvanostatic charge–discharge was performed in a potential range of 3.0–4.8 V (*vs.* Li^+/Li) using a battery cycler (TOCAT-3100, TOYO System). The C-rates were based on the theoretical capacity of the LVP (1 C = 197 mA h g^{-1}). The cyclic voltammetry (CV) was recorded at a potential range of 3.0–4.8 V at a scan rate of 0.1 mV s^{-1}. Electrochemical impedance measurement (EIS) was also conducted after the 20th charge–discharge cycle by using a Biologic VMP3 multichannel system, and the applied frequency range was from 100 kHz to 10 mHz with an amplitude of 5 mV. The typical electrode mass and thickness were about 2.5 mg cm^{-2} and 30 μm, respectively. All of the electrochemical measurements were carried out at room temperature, and all capacity values were calculated based on the weight of the LVP active material.

3. Result and discussion

Fig. 1 shows the XRD patterns of the obtained LVP composites. The sharp peaks reflect high crystallinity of the samples. All reflections can be well indexed to a monoclinic space group $P2_1$/

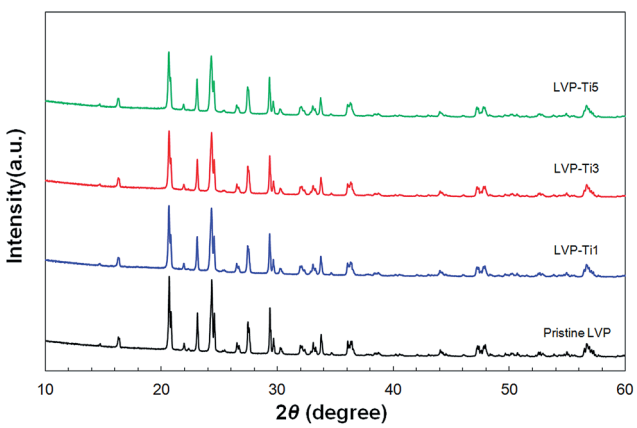

Fig. 1 XRD patterns of pristine LVP and Ti-added LVP/graphene composites.

n, indicating that TiO_2 does not influence the monoclinic structure of LVP.[11] In addition, no diffraction peaks of carbon or graphene are observed. This indicates that the carbon source is amorphous, or its content is too low to be detected. Moreover, oxalic acid and V_2O_5 were absolutely reacted in a stoichiometric ratio, implying that oxalic acid plays a role as a reducing agent in reducing V^{5+} to V^{3+} during the heat treatment process under Ar.[32] In the pristine sample, an impurity peak (Li_3PO_4) at approximately 22° is observed. It is due to either the possible loss of vanadium during the heat treatment, or excess Li source in raw materials.[33,34] However, no impurity peak is observed in Ti-added samples, indicating the high crystallinity of the LVP. It has been reported that the Ti atoms could be replaced in the vanadium site within the MO6 octahedra.[35,36] Thus, it is important to know whether the Ti atoms were substituted in the V site or disordered. In order to investigate the atomic sites in the Ti-added LVP/graphene samples, XRD pattern refinement of the pristine LVP, LVP–Ti, LVP–Ti3 and LVP–Ti5 was carried out. Fig. 2 and S1† show the refined XRD data for the Ti-added LVP/graphene samples. The calculated pattern matches well with the observed one. The refined lattice parameters and atomic coordination are listed in Table 1, S1 and S2 (see ESI†). The reliability factor χ^2 and the weighted factors R_{wp}, R_p and R_F are less than 3%; therefore, the Rietveld refinement data are expected to validate the reliable results. There is no significant deviation of the lattice parameters of Ti-added samples compared with the LVP. For example, the lattice constants *a*, *b* and *c* were 8.6102, 8.5917 and 12.0420 Å for pristine LVP and 8.6090, 8.5975 and 12.0413 Å for LVP–Ti3. Liu *et al.* reported that the formation of the three-dimensional framework of $V_2(PO_4)_3$ is dependent on the presence of carbon or graphene.[27] However, Ti-added samples in LVP/graphene do not significantly influence the lattice parameters of the LVP in our study. The Rietveld analysis did not clearly indicate that Ti substitution on the V1 or V2 site in the LVP occurred. The monoclinic unit cell of the LVP contains three independent lithium sites and redox-active metal sites.[11] The three lithium ions can be reversibly extracted or reinserted from the monoclinic structure of vanadium phosphate. From the calculated Rietveld refinement data, the atomic sites of Li, V and P of fractional coordinates in the pristine LVP, LVP–Ti1, LVP–Ti3 and LVP–Ti5 show minor deviation among the samples. Delacourt and Ellis reported that Nb and Zr do not act as internal dopant, and both elements are primarily located on the surface of the particles.[37,38] It was also reported that an excessive amount of dopants could affect the disordered structure or impurities in bulk materials.[26] Therefore, the results without any impurities in XRD data imply that Ti doping in LVP has not taken place. Elemental analysis of the residual carbon content on the Ti-added LVP was determined to be 3.12%, which is the overall carbon content, including graphene and other carbon sources.

The SEM images of all Ti-added LVP/graphene samples are shown in Fig. 3. The morphology of LVP particles is different with Ti and graphene. The pristine LVP is composed of irregular particles, and the particles are agglomerated with a broad particle size distribution. The particle size of the Ti-added LVP/graphene samples is smaller than that of the pristine LVP. For example, the LVP–Ti3 sample has a smaller particle size distribution ranging from 0.5 to 2.0 μm. The smaller particle size can shorten the diffusion path of the Li ions and enlarge the active surface area of the electrode reaction, which is advantageous for improving the electrochemical performance. The particle sizes of Ti-added LVP/graphene samples are investigated *via* particle size analyzer (Fig. S2, ESI†). The LVP–Ti3 shows the smallest particle size with an average size of 22.3 μm, whereas the pristine LVP has a much larger particle size. EDX elemental mapping studies were carried out to further investigate the distribution of each element (V, P, O and Ti) and are shown in Fig. S3 (see ESI†). The Ti element is homogeneously distributed in the LVP–Ti3 sample, which clearly shows the existence of Ti atoms. The observation, therefore, indicates the presence of Ti atoms in the LVP surface or within the grain boundaries.

Fig. 4 shows the TEM images of the pristine LVP and LVP–Ti3 samples. The pristine LVP presents a large primary particle with a size of *ca.* 30 μm. Fig. 4(b) clearly reveals the successful wrapping of graphene on the LVP surface. Compared with the conventional carbon-coated LVP, graphene-wrapped LVP has better electrochemical performance due to the high intrinsic electric conductivity of graphene. Moreover, graphene reduces

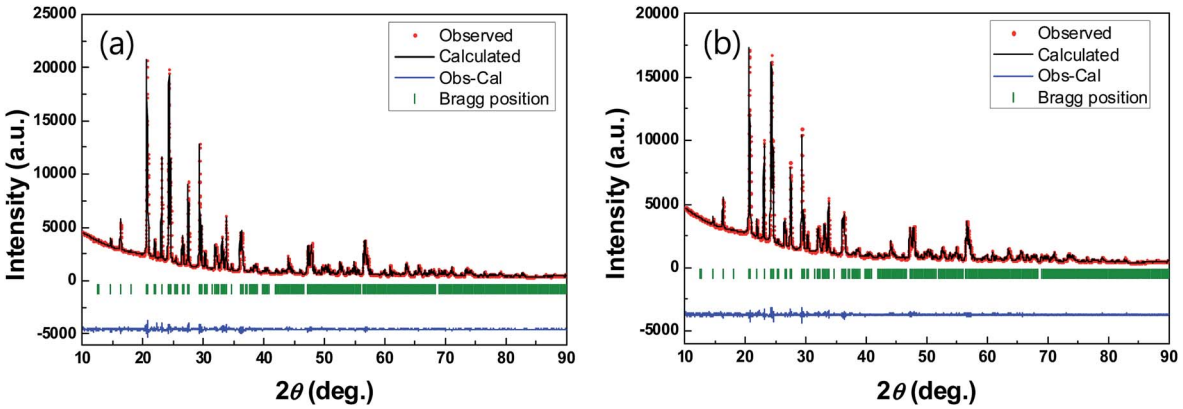

Fig. 2 Rietveld refinement XRD profiles for Ti-added LVP/graphene: (a) pristine LVP and (b) LVP–Ti3.

Table 1 Lattice parameters of pristine LVP and LVP–Ti1, LVP–Ti3 and LVP–Ti5 samples

	a (Å)	b (Å)	c (Å)	Beta (°)	Vol. (Å^3)
LVP	8.61024(2)	8.595176(18)	12.04207(2)	90.59051(4)	891.14(2)
LVP–Ti1	8.608755(9)	8.595864(9)	12.040598(12)	90.57299(3)	890.96(3)
LVP–Ti3	8.60900(5)	8.59754(3)	12.04134(3)	90.55836(3)	891.21(3)
LVP–Ti5	8.60683(5)	8.59820(3)	12.03926(4)	90.52826(14)	890.91(3)

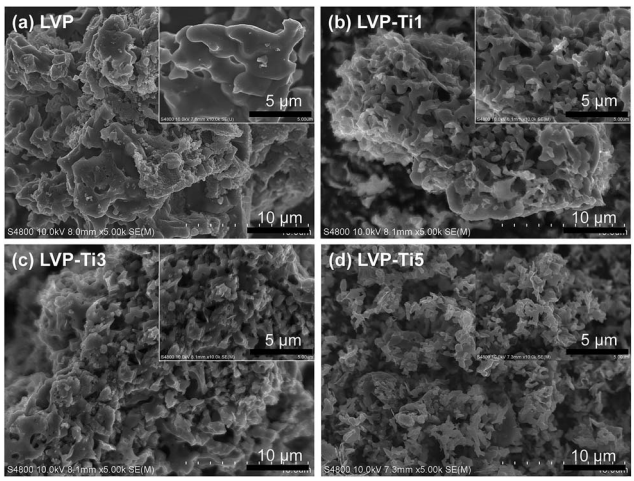

Fig. 3 SEM images of Ti-added LVP/graphene: (a) pristine LVP, (b) LVP–Ti1, (c) LVP–Ti3 and (d) LVP–Ti5.

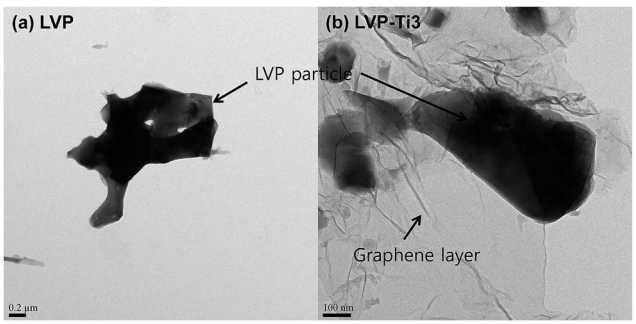

Fig. 4 TEM images of the pristine LVP (a) and LVP–Ti3 (b).

the LVP particle size and prevents the agglomeration of the LVP during the sintering process.

In order to investigate the change of chemical environment by adding Ti in LVP/graphene, XPS analysis was conducted to determine the oxidation states of V, Ti, C and O of the materials and is illustrated in Fig. 5. The scale of binding energy was calibrated according to the binding energy of the C1s peak at 284.8 eV. It is reported that the oxidation state of vanadium and titanium in the Ti-doped LVP sample is typically 3+ and +4,[35,36] respectively. In our XPS study, however, V2p has shown two peaks at 516.5 eV and 522.7 eV, which is assigned to the V2p$_{3/2}$ and V2p$_{1/2}$.[39,40] The Ti(2p$_{3/2}$) XPS showed a single peak at 454.2 eV. The XPS peak at 454.2 eV indicates the binding energy of Ti2p$_{3/2}$ in TiN from other XPS studies.[41,42] The oxidation state of V in Ti-added LVP is +4, which is higher than V^{3+}.[36] It is reported that the Ti and Mg co-doped LVP sample can partially be compensated by the higher oxidation state of vanadium.[36] This indicates that the oxidation state of vanadium could be changed from V^{3+} to V^{4+} or V^{5+} in order to maintain the charge neutrality in Ti-added LVP because of the substitution of the higher oxidation state of vanadium. As we know, XPS analysis can only detect the surface and provide information on the chemical oxidation state of elements. Combined with XPS and XRD results, we conclude that the titanium addition could lead to a shift to a higher binding energy of vanadium, and it is reasonable to consider that V^{4+} ions are formed due to the Ti^{+} ion on the surface of LVP, not inside the form of LVP.

The presence of carbon content in Ti-added LVP/graphene was observed by Raman spectroscopy. As shown in Fig. 6, there are two intense broad peaks at 1345 cm^{-1} and 1585 cm^{-1}, which correspond to the D-band (disorder-induced phonon mode) and G-band (E_{2g} vibration of graphite) of carbon, respectively.[43] The presence of D-band and G-band indicates the existence of graphite-like carbon. The intensity ratio of I_D to I_G band (I_D/I_G) of LVP–Ti1, LVP–Ti3 and LVP–Ti5 is 1.06, 1.03 and 1.04, respectively. The lower the intensity ratio, the higher the electric conductivity of the graphene.[44,45] Therefore, the electric conductivity of the LVP–Ti3 sample is expected to be the highest among the samples, resulting in the best electrochemical performance. The peaks denoted by stars in Fig. 6 indicate the vibration of $Li_3V_2(PO_4)_3$.[46] These results well agree with four-probe measurement data. The conductivity was measured in three different regions, and average electric conductivity was calculated. The electric conductivity of pristine LVP, LVP–Ti1, LVP–Ti3 and LVP–Ti5 was 2.46×10^{-4}, 2.26×10^{-4}, 1.93×10^{-3} and 2.01×10^{-4} S cm^{-1}, respectively.

CV measurement was carried out at a scan rate of 0.1 mV s^{-1} to understand the electrochemical behavior of the pristine and Ti-added LVP/graphene samples. We compared the second cycle of the CV profile, since the electrolyte penetration into the electrode, structure change and solid electrolyte interface (SEI) formation could be completed within the second cycle.[47] Fig. 7 shows the CV profiles of Ti-added LVP/graphene samples in the potential range of 3.0–4.8 V, and it is apparent that the CV curves, except for pristine LVP, are very similar. There are four oxidation peaks and three reduction peaks, corresponding to the relative Li^{+} ion extraction and reinsertion. The difference in oxidation and reduction peaks is attributed to the initial Li^{+} ion in $V_2(PO_4)_3$, which is in a solution of two phases during discharge.[11,14,48] Compared with the pristine LVP, the Ti-added LVP/graphene samples show higher and distinct current peaks. Moreover, Ti-added LVP/graphene samples present

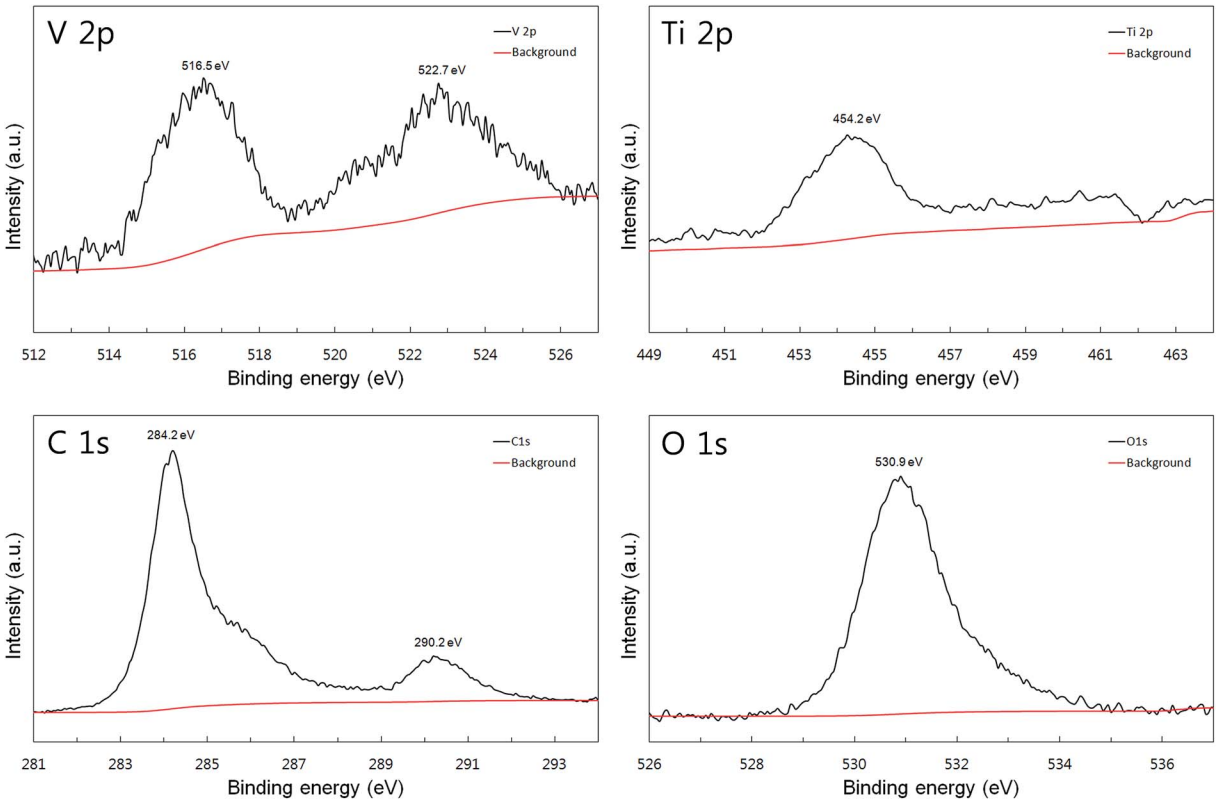

Fig. 5 XPS spectra of V2p, Ti2p, C1s and O1s in the LVP–Ti3 electrode.

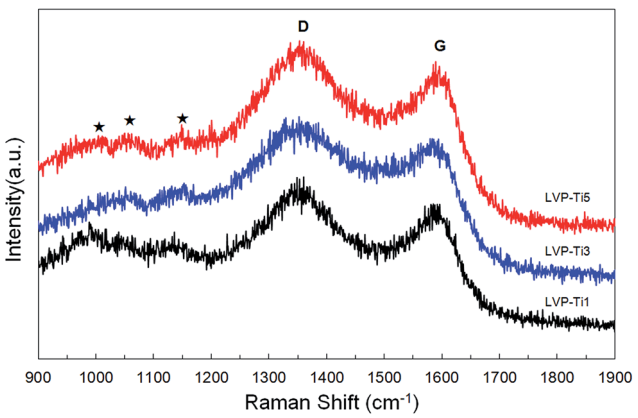

Fig. 6 Raman spectra of LVP–Ti1, LVP–Ti3 and LVP–Ti5 composites.

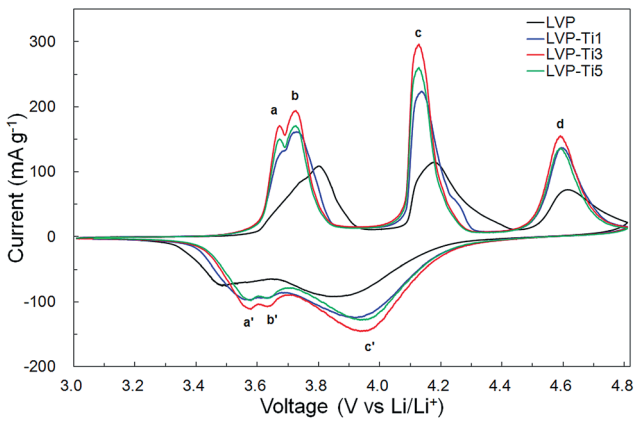

Fig. 7 CV curves of the pristine LVP, LVP–Ti1, LVP–Ti3 and LVP–Ti5 composites.

smaller potential differences between anodic and cathodic peaks, indicating the good reversibility of the Li^+ ion extraction/reinsertion and lower ohmic resistance in the electrode. According to the Randles–Sevcik equation, $I_p = 2.69 \times 10^5 n^{3/2} A D^{1/2} v^{1/2} C$ (I_p is the CV peak current, n is the number of the electrons, A is the electrode area, D is the Li^+ diffusion coefficient, v is the potential scan rate, and C is the shuttle concentration),[49] the higher the peak current, the larger the Li^+ diffusion coefficient. On the basis of the CV measurement, the LVP–Ti3 electrode exhibits a well-defined, highest peak current and Li^+ ion diffusion coefficient.

In order to evaluate the electrochemical performance, the pristine and Ti-added LVP/graphene composite was galvanostatically charged and discharged in the potential range of 3.0–4.8 V. Fig. 8 shows the first charge–discharge curves of the pristine LVP and LVP–Ti1, LVP–Ti3 and LVP–Ti5 composites at 0.1 C. As shown in Fig. 8, all the composites obviously showed three charge and discharge plateaus, which are identified as the two-phase transition processes during electrochemical reactions.[9,11,12,50] The first oxidation peaks around 3.6 and 3.7 V correspond to the removal of the first Li^+ ion in two steps. The

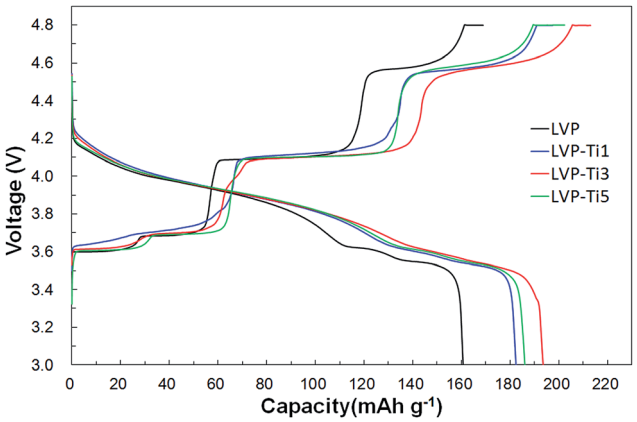

Fig. 8 First charge–discharge profiles of the pristine LVP, LVP–Ti1, LVP–Ti3 and LVP–Ti5 electrodes at 0.1 C.

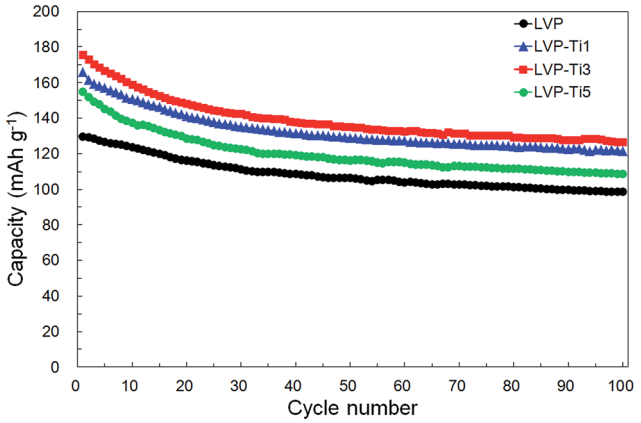

Fig. 9 Cycling performance of the pristine LVP, LVP–Ti1, LVP–Ti3 and LVP–Ti5 electrodes at 0.5 C.

second Li^+ ion is extracted at around 4.1 V, corresponding to the oxidation of V^{3+} to V^{4+}. The oxidation peak at 4.6 is the extraction of the third Li^+ ion, associated with the phase transition from $LiV_2(PO_4)_3$ to $V_2(PO_4)_3$. Even though all the composites show a similar voltage profile, the capacities of Ti-added LVP/graphene are higher than pristine LVP. In addition, the voltage difference is smaller than pristine LVP, resulting from the lower electrode polarization. The initial discharge capacity of LVP–Ti3 is 194 mA h g^{-1}, which is higher than 160, 182 and 186 mA h g^{-1} for pristine LVP, LVP–Ti1 and LVP–Ti5, respectively. This capacity value of LVP–Ti3 is close to the theoretical value of 197 mA h g^{-1}.

A high C-rate performance is an important factor in making high-powered, fast Li ion batteries. The rate capability of all the composites was also investigated at different current rates from 0.1 C to 10 C (Fig. S4†). With the high current rate, the voltage profiles become gradually indistinct due to electrode polarization. It is noticed that the rate capability of the LVP–Ti3 composite is higher than other composites. LVP–Ti3 delivered the highest discharge capacities of 194, 183, 176, 166, 155, 139 and 124 mA h g^{-1} at current rates of 0.1, 0.2, 0.5, 1, 2, 5 and 10 C, respectively. The extraction of three Li ions in a wide voltage window (3.0–4.8 V) results in a slight expansion of the unit cells of $V_2(PO_4)_3$ compared with $LiV_2(PO_4)_3$.[48] Moreover, there are some inevitable capacity losses due to electrolyte oxidation and electrode decomposition when the three Li ions are re-inserted in the discharge reaction. We conclude that the enhanced rate capability with graphene and Ti evidences good structure stability and better electrochemical performance at high current rates.

Capacity retention of the pristine LVP, LVP–Ti1, LVP–Ti3 and LVP–Ti5 *versus* cycle number was investigated. The cycling test was conducted at 0.5 C after 2 cycles at 0.1 C and recorded at the third cycle. As shown in Fig. 9, LVP–Ti3 shows the best electrochemical performance among the samples. The initial specific capacity of LVP–Ti3 at 0.5 C is 175 mA h g^{-1}, whereas the specific capacity of the pristine LVP is 129 mA h g^{-1}, which is much higher than pristine LVP. After 100 cycles at 0.5 C, however, the capacity retention ratio of the pristine, LVP–Ti1, LVP–Ti3 and LVP–Ti5 was 76, 73, 72 and 70%, respectively, indicating that the capacity fading of the Ti-added LVP/graphene samples is faster than that of the pristine LVP. This is probably due to the instability of the carbonate-based electrolyte at 4.8 V. The reason for the relatively poor capacity retention ratio is as follows. First, progressive dissolution of vanadium in electrolyte and/or electrolyte decomposition at high voltage may have occurred. Second, Ti addition can change the cation distribution and cause structure deformation during the cycle, which will lower the utilization of V.[36] Third, as-obtained Ti-added LVP/graphene cannot prevent the widespread problem of peeling off or adhesion of the LVP particles on graphene sheets. Detailed study is needed to deal with this phenomenon, which can improve the capacity retention at initial cycles.

We have also investigated the effect of different amounts of graphene in the LVP–Ti3 composite. The charge–discharge profile of LVP–Ti3 with different graphene amounts is depicted in Fig. S4.† The carbon content in LVP–Ti3 detected by the elemental analyzer was 1.2, 3.0 and 7.1 wt%, respectively. As shown in Fig. S5,† the discharge capacity of LVP–Ti3 with 1.2, 3.0 and 7.1 wt% of graphene are found to be 183, 194 and 167 mA h g^{-1}, respectively. The above result indicates that 3.0 wt% graphene in LVP exhibits a higher discharge capacity compared with those of 1.2 and 7.1 wt% graphene. Typically, specific capacity could be improved as a function of increasing carbon content. However, our observed result is not linear with increasing carbon content. We concluded that the graphene amount in LVP is a critical factor in determining the electrochemical performance of Ti-added LVP/graphene composite, and the graphene amount of 3.0 wt% is the optimum content to achieve exceptional electrochemical performance.

EIS analysis of Ti-added LVP/graphene composites was conducted at the same discharge state after 20 cycles at 0.5 C (Fig. 10). The EIS profiles of all the samples are shown as semicircles and an inclined line. The intercept on Z_{re} in the high-frequency region corresponds to the contact resistance of the electrolyte and electrode (R_e), which are almost the same. A semicircle in the high-frequency region corresponds to the

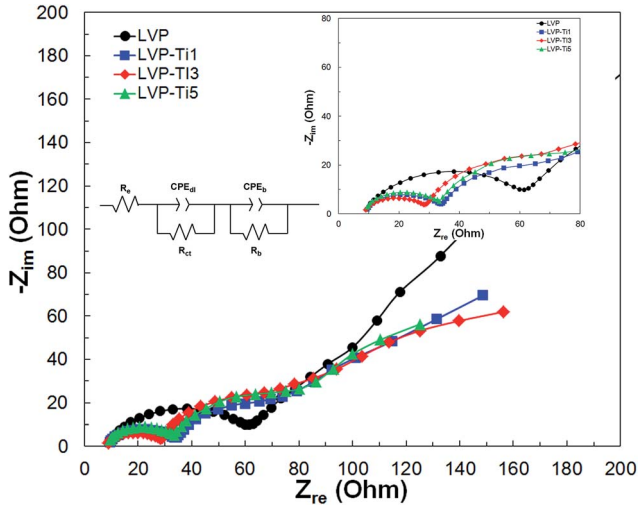

Fig. 10 EIS spectra of the pristine LVP, LVP–Ti1, LVP–Ti3 and LVP–Ti5 electrodes after 20 cycles.

contact resistance at the electrode/electrolyte interface and the double-layer capacitance between the electrolyte and cathode. The straight line in the low-frequency region is assigned to the lithium ion diffusion process within the electrodes.[51,52] The higher charge resistance indicates the slower the kinetics of the electrodes. As shown in Fig. 10, all of the Ti-added LVP/graphene samples show lower R_{ct} value than that of the pristine LVP, implying that the electrode possesses a high electric conductivity and a rapid charge-transfer reaction due to the smaller particle size, graphene and Ti elements. Compared with the pristine LVP, LVP–Ti3 shows the lowest R_{ct} value of 28 Ω, indicating a faster kinetics for electrochemical reactions. After 20 cycles, there are broad semicircles at the medium-frequency region. It is mainly attributed to the interface reaction between the electrode and the electrolyte. As described in the cycle performance, the carbonate electrolyte can decompose at high voltage, which results in a side reaction between the graphene and electrolyte. This is consistent with the significant capacity fading at the initial cycle in Fig. 9. A more detailed study of the capacity fading at initial cycle is currently underway.

Based on the above observations, our study implies that the Ti-added LVP/graphene composites show both high specific capacity and rate capability. Our result is comparable with that of reported metal-doped LVP/C.[18–21] The possible reason for this finding is as follows: first, the addition of titanium and graphene did not affect the crystal structure of LVP without impurity, and the size of the primary particle is significantly decreased, resulting in the large surface area of the LVP electrode. Second, the conductive materials of both graphene and titanium atoms improve the electrical conductivity of the Ti-added LVP/graphene composites, thus providing the electronic conductive network for fast electron transport in the graphene and titanium matrix. Third, the large surface area of Ti-added LVP/graphene makes more electron pathways and better contact with the electrolyte, which is favorable for high rate capabilities. It can be observed from the EIS measurement that the charge transfer resistance was significantly decreased compared with the pristine LVP. Furthermore, the amount of graphene is optimal for fast electron transport in order to maximize the specific capacity of Ti-added LVP/graphene composite. Thus, the 3 wt% graphene in Ti-added LVP is desirable to facilitate electron conductivity and improve the electrochemical behavior.

4. Conclusion

In summary, we have synthesized Ti-added LVP/graphene composites *via* a facile route. Physical measurement using XRD, SEM, TEM, XPS, and Raman spectroscopy indicates that the Ti-added LVP/graphene composite has fewer impurities and has a smaller particle size compared to the pristine LVP. In addition, the oxidation state of V is 4+ because of the Ti addition, and V^{4+} ions are formed on the surface of LVP, not inside the form of LVP. In the electrochemical test, LVP–Ti3 exhibits the best specific capacity of 194 mA h g^{-1} at 0.1 C in the potential range of 3.0–4.8 V. The Ti-added LVP/graphene composites also show higher rate capability and cycle performance compared with the pristine LVP. This is mainly attributed to the smaller particle size and the electron conducting network with graphene and titanium elements. In addition, 3.0 wt% of graphene is optimal to maximize the specific capacity at 0.1 C. The conducting matrix of graphene and titanium could play a critical role in decreasing the charge transfer resistance of Ti-added LVP/graphene composites. Finally, our results indicate that the synthesis is easy and expected to be applicable for other phosphate-based cathode materials in advanced lithium-ion batteries.

Acknowledgements

This work was supported by the Industrial Strategic Technology Development Program (10045401, development of high-voltage multi-transition metal phosphate cathode material) funded by the Ministry of Trade, Industry & Energy (MOTIE, Korea) and the KERI Primary Research Program of MSIP/ISTK (no. 14-12-N0101-69).

References

1 N. Recham, J.-N. Chotard, L. Dupont, C. Delacourt, W. Walker, M. Armand and J.-M. Tarascon, *Nat. Mater.*, 2010, **9**, 68–74.
2 J. M. Tarascon, *Nat. Chem.*, 2010, **2**, 510.
3 J. M. Tarascon and M. Armand, *Nature*, 2008, **451**, 652–657.
4 R. V. Chebiam, F. Prado and A. Manthiram, *Chem. Mater.*, 2001, **13**, 2951–2957.
5 A. K. Padhi, K. S. Nanjundaswamy and J. B. Goodenough, *J. Electrochem. Soc.*, 1997, **144**, 1188–1194.
6 J. Wolfenstine and J. Allen, *J. Power Sources*, 2005, **142**, 389–390.
7 J. Yang and J. J. Xu, *J. Electrochem. Soc.*, 2006, **153**, A716–A723.

8 H. H. Li, J. Jin, J. P. Wei, Z. Zhou and J. Yan, *Electrochem. Commun.*, 2009, **11**, 95–98.
9 M. Y. Saidi, J. Barker, H. Huang, J. L. Swoyer and G. Adamson, *J. Power Sources*, 2003, **119–121**, 266–272.
10 H. Huang, S.-C. Yin, T. Kerr, N. Taylor and L. F. Nazar, *Adv. Mater.*, 2002, **14**, 1525–1528.
11 S.-C. Yin, H. Grondey, P. Strobel, M. Anne and L. F. Nazar, *J. Am. Chem. Soc.*, 2003, **125**, 10402–10411.
12 S.-C. Yin, H. Grondey, P. Strobel, H. Huang and L. F. Nazar, *J. Am. Chem. Soc.*, 2003, **125**, 326–327.
13 X. Du, W. He, X. Zhang, Y. Yue, H. Liu, X. Zhang, D. Min, X. Ge and Y. Du, *J. Mater. Chem.*, 2012, **22**, 5960–5969.
14 M. Y. Saidi, J. Barker, H. Huang, J. L. Swoyer and G. Adamson, *Electrochem. Solid-State Lett.*, 2002, **5**, A149–A151.
15 A. S. Arico, P. Bruce, B. Scrosati, J. M. Tarascon and W. Van Schalkwijk, *Nat. Mater.*, 2005, **4**, 366–377.
16 H. Li and H. Zhou, *Chem. Commun.*, 2012, **48**, 1201–1217.
17 Y. Wang, H. Li, P. He, E. Hosono and H. Zhou, *Nanoscale*, 2010, **2**, 1294–1305.
18 M. Ren, Z. Zhou, X. Gao, W. Peng and J. Wei, *J. Phys. Chem. C*, 2008, **112**, 5689–5693.
19 S. Xun and J. Chong, *J. Mater. Chem.*, 2012, **22**, 15775–15781.
20 L. Zhang, G. Liang, G. Peng, F. Zou, Y. H. Huang, M. C. Cro and A. Ignatov, *J. Phys. Chem. C*, 2012, **116**, 12401–12408.
21 H. Liu, P. Gao, J. Fang and G. Yang, *Chem. Commun.*, 2011, **47**, 9110–9112.
22 J. Barker, R. K. B. Gover, P. Burns and A. Bryan, *J. Electrochem. Soc.*, 2007, **154**, A307–A313.
23 M. Ren, Z. Zhou, Y. Z. Li, X. P. Gao and J. Yan, *J. Power Sources*, 2006, **162**, 1357–1362.
24 Y. Chen, Y. Zhao, X. An, J. Liu, Y. Dong and L. Chen, *Electrochim. Acta*, 2009, **54**, 5844–5850.
25 C. S. Dai, Z. Y. Chen, H. Z. Jin and X. G. Hu, *J. Power Sources*, 2010, **195**, 5775–5779.
26 Q. Kuang, Y. Zhao, X. An, J. Liu, Y. Dong and L. Chen, *Electrochim. Acta*, 2010, **55**, 1575–1581.
27 S. Q. Liu, S. C. Li, K. L. Huang and Z. H. Chen, *Acta Phys.–Chim. Sin.*, 2007, **23**, 537–542.
28 H. Liu, G. Yang, X. Zhang, P. Gao, L. Wang, J. Fang, J. Pinto and X. Jiang, *J. Mater. Chem.*, 2012, **22**, 11039–11047.
29 B. Pei, Z. Jiang, W. Zhang, Z. Yang and A. Manthiram, *J. Power Sources*, 2013, **239**, 475–482.
30 K. Wu and J. Yang, *Mater. Res. Bull.*, 2013, **48**, 435–439.
31 M. Choi, H. Kim, Y. lee and B. Jin, *J. Mater. Chem.*, 2014, **2**, 7873–7879.
32 Y. H. Jung, C. H. Lim and D. K. Kim, *J. Mater. Chem. A*, 2013, **1**, 11350–11354.
33 L. Fei, W. Lu, L. Sun, J. Wang, J. Wei, H. L. W. Chan and Y. Wang, *RSC Adv.*, 2013, **3**, 1297–1301.
34 C. Wang, H. Liu and W. Yang, *J. Mater. Chem.*, 2012, **22**, 5281–5285.
35 Y. G. Mateyshina and N. F. Uvarov, *J. Power Sources*, 2011, **196**, 1494–1497.
36 C. Deng, S. Zhang, S. Y. Yang, Y. Gao, B. Wu, L. Ma, B. L. Fu, Q. Wu and F. L. Liu, *J. Phys. Chem. C*, 2011, **115**, 15048–15056.
37 C. Delacourt, C. Wurm, L. Laffont, J.-B. Leriche and C. Masquelier, *Solid State Ionics*, 2006, **177**, 333–341.
38 B. Ellis, P. S. Herle, Y.-H. Rho, L. F. Nazar, R. Dunlap, L. K. Perry and D. H. Ryan, *Faraday Discuss.*, 2007, **134**, 119–141.
39 S. Zhnag, Q. Deng, F. L. Liu, M. Zhang, F. L. Meng and H. Gao, *J. Power Sources*, 2012, **218**, 56–64.
40 C. S. Sun, Z. Zhou, Z. G. Xu, D. G. Wang, J. P. Wei, X. K. Bian and J. Yan, *J. Power Sources*, 2009, **193**, 841–845.
41 *Handbook of X-ray Photoelectron Spectroscopy*, ed. G. D. Wagner, W. M. Riggs, L. E. Davis, J. F. Moulder and G. E. Muilernberg, Perkin-Elmer, Eden Prairie, MN, 1979.
42 L. Porte, L. Roux and J. Hanns, *Phys. Rev.*, 1983, **28B**, 3214–3224.
43 A. Ferrari and J. Robertson, *Phys. Rev. B: Condens. Matter Mater. Phys.*, 2000, **61**, 14095–14107.
44 J. W. Wang, J. Liu, G. L. Yang, X. F. Zhang, X. D. Yan, X. M. Pan and R. S. Wang, *Electrochim. Acta*, 2009, **54**, 6451–6454.
45 Y. Q. Qiao, J. P. Tu, X. L. Wang, D. Zhang, J. Y. Xiang, Y. J. Mai and C. D. Gu, *J. Power Sources*, 2011, **196**, 7715–7720.
46 C. M. Burba and R. Frech, *Solid State Ionics*, 2007, **177**, 3445–3454.
47 X. Zhou, Y. Liu and Y. Guo, *Electrochim. Acta*, 2009, **54**, 2253–2258.
48 S. Patoux, C. Wurm, M. Morcrette, G. Rousse and C. Masquelier, *J. Power Sources*, 2003, **119**, 278–284.
49 L. L. Zhang, G. Liang, A. Ignatov, M. C. Croft, X. Q. Xiong, I. M. Hung, Y. H. Huang, X. L. Hu, W. X. Zhang and Y. L. Peng, *J. Phys. Chem. C*, 2011, **115**, 13520–13527.
50 H. Huang, S. C. Yin, T. Kerr, N. Taylor and L. F. Nazar, *Adv. Mater.*, 2002, **14**, 1525–1528.
51 J. Jamnik and J. Maier, *J. Electrochem. Soc.*, 1999, **146**, 4183–4188.
52 S. B. Yang, H. H. Song and X. H. Chen, *Electrochem. Commun.*, 2006, **8**, 137–142.